The SCUBA 8-mJy survey - II. Multiwavelength analysis of bright submillimetre sources

Article (Published Version)

Mon. Not. R. Astron. Soc. **331,** 839–852 (2002)

The SCUBA 8-mJy survey – II. Multiwavelength analysis of bright submillimetre sources

M. J. Fox,[1★] A. Efstathiou,[1] M. Rowan-Robinson,[1] J. S. Dunlop,[2] S. Scott,[2] S. Serjeant,[1,7] R. G. Mann,[1,2] S. Oliver,[1,8] R. J. Ivison,[3] A. Blain,[4,9] O. Almaini,[3] D. Hughes,[5] C. J. Willott,[6] M. Longair,[4] A. Lawrence[2] and J. A. Peacock[2]

[1]*Astrophysics Group, Blackett Laboratory, Imperial College of Science Technology & Medicine, Prince Consort Road, London SW7 2BW*
[2]*Institute for Astronomy, University of Edinburgh, Royal Observatory, Blackford Hill, Edinburgh EH9 3HJ*
[3]*UK ATC, Royal Observatory, Blackford Hill, Edinburgh EH9 3HJ*
[4]*Institute of Astronomy, Madingley Road, Cambridge CB3 0HA*
[5]*Instituto Nacional de Astrofisica, Optica y Electronic (INAOE), Apartado Postal 51 y 216, 72000 Puelba, Pue., Mexico*
[6]*Astrophysics, Department of Physics, Keble Road, Oxford OX1 3RH*
[7]*Unit for Space Sciences and Astrophysics, School of Physical Sciences, University of Kent, Canterbury, Kent CT2 7NZ*
[8]*School of Chemistry, Physics & Enviromental Science, University of Sussex, Falmer, Brighton BN1 9QJ*
[9]*Astronomy Department, California Institute of Technology, Pasadena, CA 91125, USA*

Accepted 2001 November 1. Received 2001 November 1; in original form 2001 August 1

ABSTRACT

We present the results of a multiwavelength study of the 19 most significant submillimetre (submm) sources detected in the SCUBA 8-mJy survey. As described in Scott et al., this survey covers $\simeq 260\,\mathrm{arcmin}^2$ using the submillimetre camera SCUBA, to a limiting source detection limit $S_{850\,\mu\mathrm{m}} \simeq 8\,\mathrm{mJy}$. One advantage of this relatively bright flux-density limit is that accurate astrometric positions are potentially achievable for every source using existing radio and/or millimetre-wave interferometers. However, an associated advantage is that spectral energy distribution (SED) based redshift constraints should be more powerful than in fainter submm surveys. Here we therefore exploit the parallel SCUBA 450-μm data, in combination with existing radio and *Infrared Space Observatory* (*ISO*) data at longer and shorter wavelengths to set constraints on the redshift of each source. We also analyse new and existing optical and near-infrared imaging of our SCUBA survey fields to select potential identifications consistent with these constraints. Our derived SED-based redshift constraints, and the lack of statistically significant associations with even moderately bright galaxies allow us to conclude that all 19 sources lie at $z > 1$, and at least half of them apparently lie at $z > 2$.

Key words: galaxies: distances and redshifts – galaxies: evolution – galaxies: starburst – cosmology: observations.

1 INTRODUCTION

Even prior to the advent of the first major submillimetre (submm) surveys it was anticipated that, if substantial numbers of sources were to be uncovered by surveys conducted at 850 μm, the vast majority of these would most probably lie at high redshift $z > 1$ (Blain & Longair 1996; Hughes & Dunlop 1998). This is a simple consequence of the realization that the present-day *IRAS* luminosity function needs to be subjected to strong cosmological evolution (comparable to that displayed by powerful active galactic nuclei, AGN, out to $z \simeq 2$) in order to yield a significant number of sources in currently feasible 850-μm surveys.

However, while a series of surveys with the Submillimetre Common User Bolometer Array (SCUBA) on the James Clerk Maxwell Telescope (JCMT) have now confirmed the existence of large numbers of submm sources (Smail, Ivision & Blain 1997; Hughes et al. 1998; Barger et al. 1998; Eales et al. 1999; Blain et al. 1999; Barger, Cowie & Sanders 1999a), actually measuring or even constraining the redshift distribution of this important extragalactic population is proving extremely difficult. There are a number of reasons for this, perhaps the most obvious of which is that very few of these sources transpire to be associated with observable AGN emission (Fabian et al. 2000; Hornschemeier et al. 2000; Barger

★E-mail: m.fox@ic.ac.uk

et al. 2001a,b). In fact, to date spectroscopic redshifts have only been measured for three of the bright submm sources uncovered by blank-field SCUBA surveys, in two cases (SMM J02399−0136 at $z = 2.8$ and SMM J02400−0134 at $z = 1.1$) aided by the (apparently) rare occurrence of detectable AGN activity (Ivison et al. 1998; Soucail et al. 1999).

Nevertheless, the situation is not quite as hopeless as is sometimes portrayed. In particular, while it is clear that the ideal of spectroscopically determined redshifts [via optical, maser line (Townsend et al. 2001), infrared (IR) or CO millimetre-wave spectroscopy] for substantial numbers of SCUBA sources remains a distant goal, much effort has been invested in refining techniques of redshift estimation which can be implemented with the current instrumentation (see Dunlop 2001 for an overview).

In practice, four key steps can be identified along the route towards establishing an unambiguous redshift for a submm source. These are as follows.

(i) Establish an allowed redshift range consistent with the observed radio-to-infrared spectral energy distribution (SED) of the source.

(ii) Identify possible candidate optical/IR counterparts consistent both with the position of the SCUBA source and with the SED-based redshift constraints.

(iii) Establish which (if any) of the potential optical/IR identifications is the correct one through improved astrometry provided by deep radio or millimetre interferometry.

(iv) Given a trustworthy optical/IR identification, measure its spectroscopic redshift.

It is already clear that attempting to short-circuit this sequence and jump straight to step (iv) (i.e. measure a redshift for all potential optical/IR counterparts) not only represents very expensive use of valuable large-telescope time, but can produce potentially misleading results (Barger et al. 1999b). Indeed, given the faintness and redness of some of the optical/IR counterparts, there is a serious possibility that spectroscopic redshifts may not prove measurable for a substantial fraction of SCUBA sources until the advent of the *Next Generation Space Telescope* (*NGST*) and/or the Atacama Large Millimetre Array (ALMA).

It is therefore important to recognize the value of steps (i) to (iii) in the above sequence, and to attempt to maximize the undoubted potential of such currently feasible measurements for establishing the basic nature of the submm source population.

To date, the effectiveness of step (i) (i.e. SED-based redshift constraints) has been hampered by the lack of sufficiently bright submm sources revealed by existing surveys. For example, only three of the 850-μm sources uncovered by the SCUBA surveys of the *Hubble Deep Field* HDF-N proper (Hughes et al. 1998; Serjeant et al. 2002) and of the 14-hr field of the Canada–France Redshift Survey (CFRS; Eales et al. 2000) have $S_{850} > 5$ mJy, and obtaining complementary detections of the fainter sources at either 450 μm or 1.4 GHz has, unsurprisingly, proved to be extremely difficult (Eales et al. 2000).

Fortunately, the recently completed '8-mJy' SCUBA survey has transformed this situation, yielding 36 sources with $S_{850} > 5$ mJy and a signal-to-noise ratio (S/N) > 3.5 (Scott et al. 2002, this issue). In this paper we report the first results of attempting steps (i) and (ii) for the 19 most significant ($>4\sigma$) of these sources. An important feature of this new SCUBA-selected sample is that all of the sources are bright enough to be detectable with existing radio and/or millimetre interferometers (e.g. Downes et al. 1999; Gear et al. 2000). Thus, ultimately, we would anticipate that step (iii) in the above procedure can also be completed for the bulk of this new submm sample (Lutz et al. 2001; Ivison et al., in preparation).

Here we focus on what can be deduced about these sources from the existing multifrequency data available for the 8-mJy survey fields. This survey has the advantage of deep multiwavelength data from the European Large Area *ISO* Survey (ELAIS) project (Oliver et al. 2000) for 50 per cent of the total area at 7, 15, 90 and 175 μm. The remaining 50 per cent is covered with other *ISO* observations. There also exists a wealth of available data in the *I* and *R* bands (Willott et al., in preparation), at X-ray wavelengths (Hasinger et al. 1998; Schmidt et al. 1998; Lehmann et al. 2000; Lehmann et al. 2001) and at 1.4 GHz (de Ruiter et al. 1999; Ciliegi et al. 1998). We have also now acquired deep *K*-band imaging of the central regions of both fields, using the United Kingdom Infrared Telescope (UKIRT) Fast Track Imager (UFTI) and the Isaac Newton Group Red Imaging Device (INGRID) on the William Herschel Telescope (WHT).

The paper is organized as follows. In Section 2 we present and analyse the parallel 450-μm SCUBA survey images. In Section 3 we then combine the resulting detections/limits with existing radio, far-infrared and millimetre-wave data to determine SED-based redshift constraints for the 19 most significant 850-μm sources. In Section 4 we exploit deep optical and near-infrared imaging of our SCUBA fields to detect and quantify the probability of candidate identifications. Finally, in Section 5 we place the main results of this work in context, discuss the significance of our principal findings, and highlight the importance of forthcoming deeper multifrequency observations of the 8-mJy SCUBA survey.

2 PARALLEL 450-μm SCUBA IMAGING

2.1 450-μm maps

The 8-mJy survey covers a total area of approximately 260 arcmin^2, divided roughly evenly between two fields; the Lockman Hole East and one of the ELAIS survey regions in the northern sky, ELAIS N2. These two survey areas were selected for their low galactic cirrus emission and the extent of pre-existing multiwavelength data. As reported by Scott et al. (2001), both survey fields have been imaged at $\lambda = 850$ μm with SCUBA to a typical rms noise level of $\sigma_{850} \simeq 2.2$ mJy, yielding 19 sources with S/N > 4, 38 sources with S/N > 3.5 and 72 sources with S/N > 3. The flux densities of the 19 most significant 850-μm sources which are the focus of this multifrequency analysis are restated here for ease of reference in Table 1.

Because SCUBA observes simultaneously at 450 and 850 μm, we have also obtained parallel 450-μm images of these two survey fields. The 450-μm observations are inevitably of poorer sensitivity because of the lower atmospheric transmission and lower aperture efficiency, and are also more difficult to calibrate reliably. The atmospheric opacity at 450-μm was typically less than 1.8. Mars and Uranus were used as primary calibrators with CRL618, OH231.8 and CRL2688 as secondary calibrators and were observed using a 30-arcsec chop throw identical to the survey strategy. At 450 μm we find a typical calibration error of 20 per cent. Despite this large uncertainty in the calibration, the parallel 450-μm data are of considerable value as a result of the fact that the flux-density ratio S_{850}:S_{450} is a strong function of redshift. This is because the greybody spectrum produced by a dust-enshrouded starburst galaxy rises as steeply as $f_\nu \propto \nu^{3-4}$ in the rest-frame submm, but gradually flattens at shorter wavelengths, turning over

Table 1. Table of flux densities and magnitudes (using a 1.5-arcsec radius aperture) of SCUBA detections and possible counterparts. The numbers in parentheses refer to the individual objects indicated in Tables 3 and 4.

Catalogue name	S_X [f]	m_I	m_R	m_K	$S_{7\,\mu\mathrm{m}}$ (mJy)	$S_{15\,\mu\mathrm{m}}$ (mJy)	S_{850} (mJy)	S_{450} (mJy) (or 3σ limit)	$S_{1.4\,\mathrm{GHz}}$ (mJy) (or 4σ limit)
LH850.1[a]	<3	>27.4[g]		20.78 ± 0.03	<0.1	<0.1	10.5 ± 1.6	25 ± 7	0.062 ± 0.013[h]
LH850.2	<12	22.9 ± 0.1					10.9 ± 2.4	<40	<0.28
LH850.3	<12	23.4 ± 0.1					7.7 ± 1.7	<22	<0.16
LH850.4	<12	(1) 22.47 ± 0.1		21.02 ± 0.20			8.3 ± 1.8	<33	<0.12
	<12	(2) 22.59 ± 0.1		19.27 ± 0.07			"	"	<0.12
	<12	(3) >24.5		20.86 ± 0.18			"	"	<0.12
LH850.5	<12	>24.5					8.6 ± 2.0	<26	<0.16
LH850.6	<12	23.04 ± 0.10					11.0 ± 2.6	<40	<0.12
LH850.7	<12	23.5 ± 0.1					8.1 ± 1.9	<46	<0.24
LH850.8[b]	36	(1) 20.72	21.8	17.98 ± 0.01			5.1 ± 1.3	<21	<0.12
	<12	(2) 21.78	22.4	19.64 ± 0.01			"	"	0.13 ± 0.03
	<12	(3) >24.5		20.22 ± 0.02			"	"	<0.12
LH850.11	<12	23.5 ± 0.1					13.5 ± 3.5	77 ± 20	<0.16
LH850.12	<12	(1) 22.71 ± 0.07					6.2 ± 1.6	<27	0.29 ± 0.04[c]
	<12	(2) 23.3 ± 0.13					"	"	<0.16
LH850.14	<12	>24.5					9.5 ± 2.8	<70	<0.24
LH850.16	<12	22.68 ± 0.07					6.1 ± 1.8	<27	<0.12
LH850.18	<12	(1) 23.08 ± 0.11					4.5 ± 1.3	<16	<0.12
		(2) 23.35 ± 0.14					"	"	"
N2850.1		(1) 22.7 ± 0.02	23.40 ± 0.01		<1	<2	11.2 ± 1.6	23 ± 7	<0.30
		(2) >26	26.46 ± 0.20		<1	<2	"	"	"
		(3) >26	25.95 ± 0.12		<1	<2	"	"	"
N2850.2[d]		(1) 24.76 ± 0.10		20.57 ± 0.04	<1	<2	10.7 ± 2.0	35 ± 10	<0.30
		(2) 24.82 ± 0.10		20.64 ± 0.03	<1	<2	"	"	"
		(3) >26		20.68 ± 0.03	<1	<2	"	"	"
		(4) 25.56 ± 0.21		20.96 ± 0.03	<1	<2	"	"	"
		(5) 24.66 ± 0.09		>21.5	<1	<2	"	"	"
N2850.3		(1) 25.15 ± 0.15	26.54 ± 0.19	>21.5	<1	<2	8.5 ± 2.2	<19	<0.30
		(2) >26	25.93 ± 0.12	>21.5	<1	<2	"	"	"
		(3) >26	>27.0	21.06 ± 0.04	<1	<2	"	"	"
N2850.4[e]		(1) >26	26.26 ± 0.17	>21.5	<1	<2	8.2 ± 1.7	<34	<0.33
		(2) 22.5 ± 0.01	22.68 ± 0.10	18.58 ± 0.009	<1	<2	"	"	"
		(3) >26	25.01 ± 0.13	>21.5	<1	<2	"	"	"
N2850.5		25.04 ± 0.13	25.33 ± 0.07		<1	<2	8.5 ± 2.2	<18	<0.25
N2850.7		(1) 23.51 ± 0.04	24.10 ± 0.03	19.93 ± 0.03	<1	<2	9.0 ± 2.4	<32	<0.25
		(2) >26	25.63 ± 0.97	>21.5	<1	<2	"	"	"
		(3) 24.72 ± 0.10	>27.0	20.30 ± 0.03	<1	<2	"	"	"

[a]Additional photometry: $S_{1.2\,\mathrm{mm}} = 3.8 \pm 0.5$ mJy, $S_{1.26\,\mathrm{mm}} = 3.03 \pm 0.56$ mJy, $S_{3.3\,\mathrm{mm}} < 0.6$ mJy (Lutz et al. 2001).
[b]IRAM 30-m detection at $S_{1.2\,\mathrm{mm}} = 1.56 \pm 0.32$ mJy. Source blended with LH850.1. Catalogued as <9 arcsec in size at 1.4 GHz (de Ruiter et al. 1997).
[c]Unresolved at 1.4 GHz. (de Ruiter et al. 1997).
[d]*R*-band image heavily contaminated by diffraction spike of nearby star.
[e]IRAM 30-m detection $S_{1.2\,\mathrm{mm}} = 2.59 \pm 0.42$ mJy.
[f]0.5–2.0 keV/10^{-16} ergs^{-1} cm^{-}2.
[g]1-arcsec diameter aperture (Lutz et al. 2001).
[h]Ivison et al. (in preparation).

at $\lambda \simeq 100\,\mu$m. Consequently, 450-μm detections of very bright and/or low-redshift 850-μm sources are frequently achievable (given good atmospheric transparency), and even when detections are not achieved the resulting limits on 850/450 colour provide a valuable (albeit temperature sensitive) limit on source redshift. Furthermore, the shortwave array in SCUBA has 91 pixels (cf. 37 at 850-μm) which, coupled with the smaller beamsize of the 15-m JCMT at 450 μm [full width at half maximum (FWHM) 7.3 arcsec], results in a higher resolution map which is thus less subject to the potential effects of source confusion.

In Figs 1 and 2 we present the 450-μm images of the Lockman Hole and ELAIS N2 areas for which Scott et al. (2002) have presented maps at 850 μm. We estimate that the mean 3σ limiting depths of these maps are $S_{450} \simeq 65$ mJy for the Lockman Hole area and $S_{450} \simeq 50$ mJy for the ELAIS N2 field. However, we emphasize that these sensitivities can vary by up to 80 per cent across the maps.

2.2 Source extraction

As discussed by Scott et al. (2002), we have reduced both the 850- and 450-μm data using the Interactive Data Language (IDL) pipeline developed by Serjeant et al. (2002) in order to produce uncorrelated signal and noise images. This allows the use of maximum-likelihood source-extraction techniques as discussed by Serjeant et al. (2002) and Scott et al. (2002). Application of these source-extraction methods to the 450-μm images results in one source with S/N > 4 and 15 sources with S/N > 3.5.

Four of these 450-μm sources coincide (to within the positional errors) with 850-μm sources extracted by Scott et al. from the longer wavelength images, and for this reason are almost certainly real. However, it is doubtful that any of the other purely 450-μm selected 'sources' (those without counterparts at 850 μm) can be believed. The reason for this is that while the smaller beamsize at

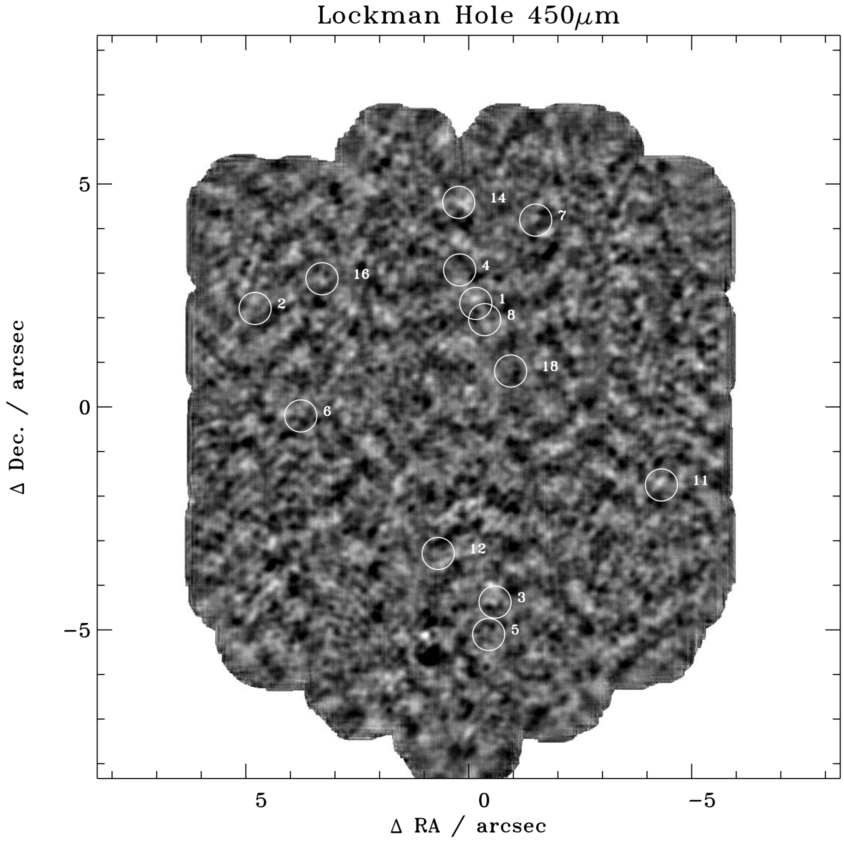

Figure 1. The 450-μm signal to noise image of the Lockman Hole region convolved with the full beam, with the locations of the 850-μm detections marked by circles. The beamsize of JCMT at 450 μm is 7.5 arcesec, producing a higher resolution image than at 850 μm. LH850.1 and LH850.11 have 450-μm counterparts and the remaining 850-μm sources have 450-μm fluxes consistent with a non-detection.

450 μm means that confusion is a less serious problem than at 850 μm, the much larger number of beams in the 450-μm maps ($\sim$5000 across the two maps) means that $\sim$22 false 'sources' with apparent S/N $>$ 3.0 are expected in these images purely on the basis of random noise. In fact, simulations of the 450-μm images of the sort undertaken by Scott et al. (2002) at 850 μm indicate that, at most, only the one ELAISN2 source with S/N $>$ 4 can be seriously considered as a possible new 450-μm selected source. At this level of significance, the expected number of false sources drop to $<$1. The position of this possible source, N2450.1, is marked in Fig. 2.

2.3 450-μm measurements of 850-μm sources

Given the relative sensitivities of the two SCUBA arrays under moderately good observing conditions, the failure of the 450-μm image to reveal any compelling new submm sources is not really surprising. The real value of these data is therefore for quantifying the 450-μm flux density of the known reliable 850-μm sources.

The positions of 19 significant 850-μm sources reported by Scott et al. (2002) are overlaid on the 450-μm images shown in Figs 1 and 2. In fact, four of the 850-μm sources are detected in the 450-μm maps with S/N $>$ 3, as judged by the most significant 450-μm peak found within 6 arcsec of each nominal 850-μm position. These detections should be taken seriously because although (as discussed above) several spurious 3σ 'sources' are expected in these maps as a result of random statistics, the probability of a spurious $>3\sigma$ 450-μm detection occurring within 6 arcsec of a known 850-μm source is very low.

These 450-μm detections are listed in column 9 of Table 1. For the remaining 13 850-μm sources indicated in Figs 1 and 2 we give conservative 3σ upper limits on S_{450} in Table 1. Both the detections and these upper limits are utilized to derive SED-based redshift estimates/constraints in the next section.

3 SED-BASED REDSHIFT CONSTRAINTS

3.1 450/850 μm flux-density ratio

For the estimation of redshift based on the submm flux-density ratio we have considered a range of model spectra similar to local ultraluminous infrared galaxies (for a review see Sanders & Mirabel 1996). Plotted in Fig. 3 are the predicted submm flux-density ratios as a function of redshift for a range of model SEDs from Efstathiou, Rowan-Robinson & Siebenmorgen (2000), produced by varying optical depth ($\tau_v = 50$–200) and starburst duration (1.7 to 72 Myr). This ensemble of model SEDs in effect spans a wide temperature range, from 'Milky Way-like' dust temperatures ($\sim$20 K) through those typically found in local luminous infrared galaxies ($\sim$35 K; Dunne, Clements & Eales 2000) and extending up to the higher temperatures displayed by some ULIRGS and HLIRGs ($\sim$50 K; Farrah et al. 2001; Dunne et al. 2000). For those sources with 450-μm detections, the S_{850}/S_{450} colour constraint provides both an upper and lower redshift limit based on comparison of the upper and lower 1σ error bounds on the measured flux-density ratio, with the locus of colour as a function of z predicted by the model ensemble. In the majority of cases the

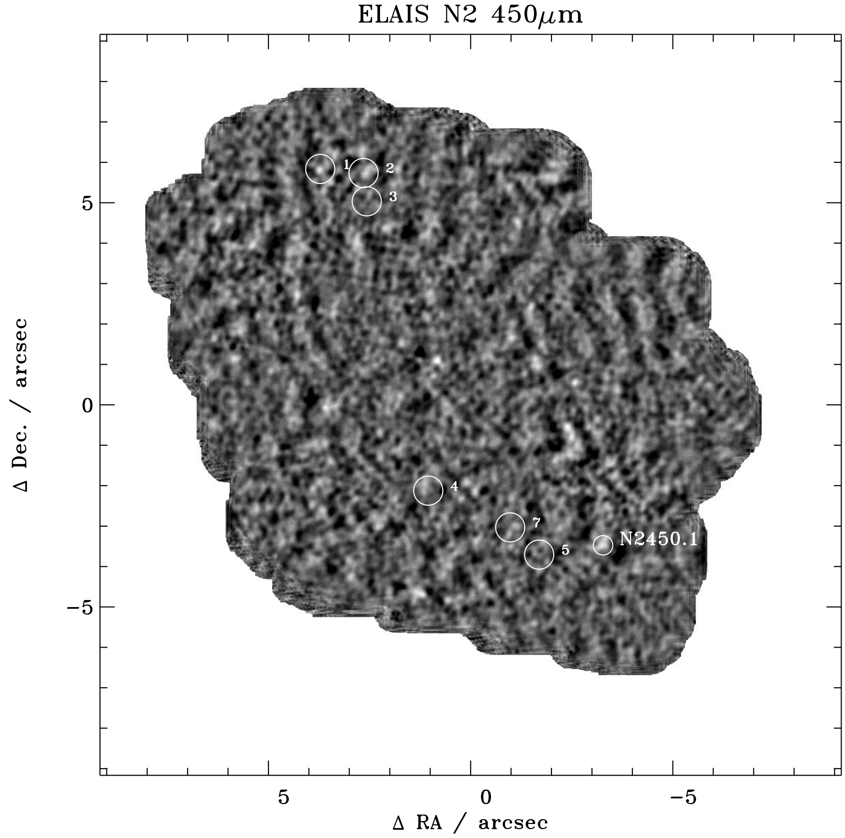

Figure 2. The 450-μm signal-to-noise ratio image of the ELAIS N2 region convolved with the full beam, with the locations of the 850-μm detections marked by circles. The two most significant sources, N2850.1 and N2850.2 have solid 450-μm detections and the remaining 850-μm sources have 450-μm fluxes consistent with a non-detection. The source N2450.1 is the one potentially real 450-μm source in the map with no significant 850-μm counterpart (see text for discussion).

850-μm sources remain undetected in the 450-μm map, in which case we simply derive a lower limit on 850/450 colour from the 3σ upper limit on S_{450} given in Table 1, and hence derive a conservative lower limit on z via comparison with the model colour locus shown in Fig. 3.

The resulting inferred redshift ranges and limits for the 19 850 μm sources are summarized in column 4 of Table 2. The ranges are wide, and the limits almost certainly conservative as a result of the wide range of model SEDs used in this analysis. However, the constraints are still sufficiently strong to conclude that the vast majority of the sources lie at $z > 1$, while at least half have redshifts $z > 2$.

Co-adding the 450-μm limits and using the mean 850-μm value for the sample yields a mean redshift lower limit for the sample of $\langle z_{\rm lim} \rangle = 1.5$, using the most conservative model SED (i.e. the upper curve in Fig. 3). Re-computing this number with an Arp 220 type SED (dashed line in Fig. 3) yields $\langle z_{\rm lim} \rangle = 2.3$.

3.2 850/1200 μm flux-density ratio

LH850.1, LH850.8 and N2850.4 have been observed at 1.2 mm using the Max Planck Millimeter Bolometer (MAMBO) instrument (Kreysa et al. 1998) at the Institut de Radioastronomie Millimétrique (IRAM) 30-m telescope. Data reduction was performed using the procedure described by Baker et al. (2001). The central photometric bolometer was centred on the 850 μm position and yielded detections at 1.2 mm for all three objects within the 11-arcsec IRAM beam. These longer wavelength measurements are of use because they can exclude very high redshifts on the basis of the resulting $S_{850\,\mu\rm m}/S_{1.2\,\rm mm}$ flux ratios. Using the same wide range of SEDs as discussed above leads to the conclusion that the measured $S_{850\,\mu\rm m}/S_{1.2\,\rm mm}$ value for LH850.1 is consistent with the redshift range $0.5 < z < 5$ taking the upper and lower 1-σ error on the observed ratio. On the same basis, LH850.8 and N2850.4 are consistent with $0 < z < 3$. These, albeit broad, redshift ranges are included in column 6 of Table 2.

3.3 Radio 20-cm data

Many of the SCUBA sources from previous surveys have been detected at radio wavelengths via deep ($3\sigma \sim 10$–100 μJy) Very Large Array (VLA) observations (Smail et al. 2000; Ivison et al. 1998, 2000; Carilli et al. 2001; Bertoldi et al. 2001) and faint radio sources have been targeted and detected by SCUBA (Barger, Cowie & Richards 2000; Chapman et al. 2001). High-resolution radio observations can provide very accurate positions for SCUBA sources, as well as yielding independent redshift estimates and morphological information. Using the tight far-IR–radio correlation for starburst galaxies Helou, Soifer & Rowan-Robinson 1985; Condon (1992), Carilli & Yun (1999, 2000) produced a redshift indicator based on the predicted redshift dependence of the observed spectral index between 20 cm and 850 μm. Dunne et al. (2000) have produced a similar radio–submillimetre redshift

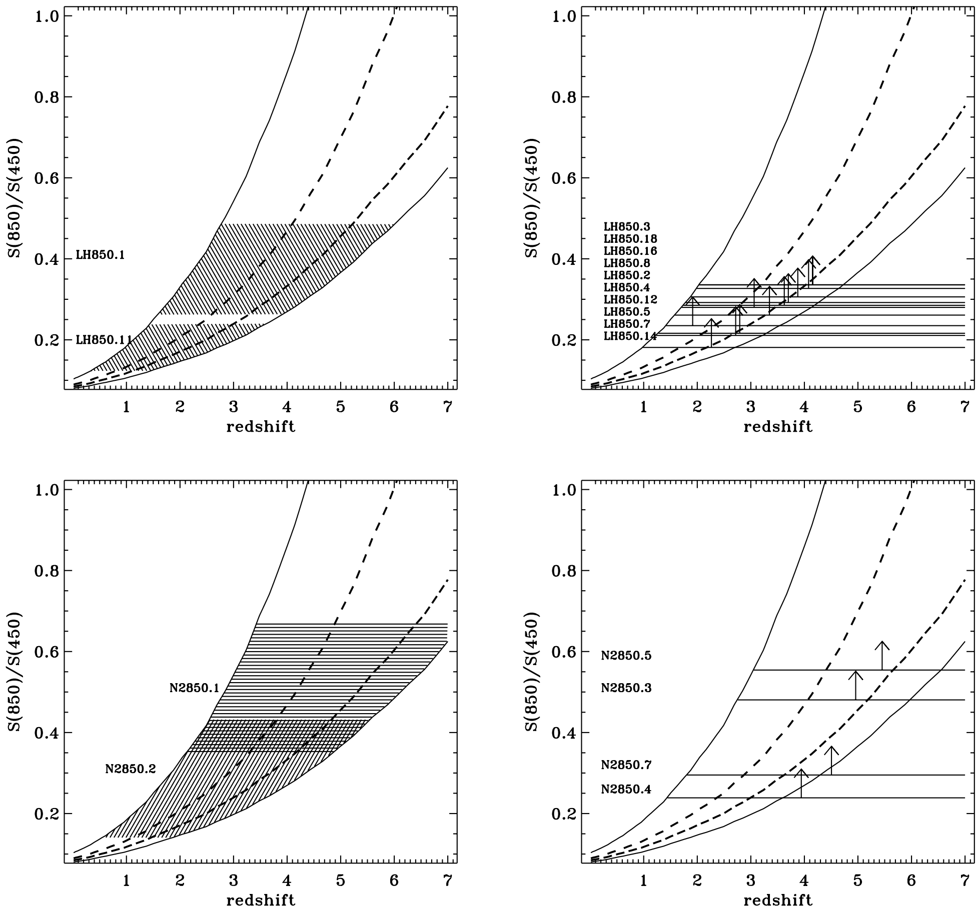

Figure 3. S_{850}/S_{450} colour–redshift constraints for the 850-μm sources in the Lockman Hole E (top panels) and ELAIS N2 (bottom panels) survey fields. The figures on the left illustrate the constraints derived for the four 850-μm selected sources which have also been detected at 450 μm. The locus bounded by the two solid curves indicates how S_{850}/S_{450} is predicted to vary with increasing z for the range of starburst models described in the text, while the dashed and dot-dashed lines are the S_{850}/S_{450} colour–redshift relations for Arp 220 and M82. The shaded regions thus indicate the range of possible redshifts for these four sources, consistent with the 1σ errors on their observed submm flux-density ratios. The figures on the right then illustrate what redshift limits can be derived for the remaining 15 850-μm sources which have only 450-μm upper limits. The ranges and limits on source redshifts derived from the comparison illustrated here are tabulated in column 4 of Table 2.

indicator based on data from a large (104-source) sample of low-redshift galaxies. Both studies suggest that values of $\alpha^{850\,\mu m}_{20\,cm} \geq +0.5$ (where $f_\nu \propto \nu^\alpha$) places sources at high redshift ($z \geq 1$). Assuming that the SCUBA sources detected in this survey have properties not dissimilar to the dust-enshrouded galaxies used in the calibration of these relations, we can expect radio flux densities $\simeq 0.1$ mJy at 20 cm. Medium-deep 20-cm surveys have been performed by Ciliegi et al. (1998) in the ELAIS N2 area to a maximum depth of 0.135 mJy (5σ) and by de Ruiter et al. (1997) in the Lockman Hole area to a comparable depth. Three sources in the Lockman Hole area (LH850.1, LH850.8 and LH850.12) have close radio associations. The remaining sources fall below the respective detection limits of the two radio surveys.

All bar one (LH850.8, but see Section 4.2 for discussion) of the SCUBA sources have $\alpha^{850\,\mu m}_{20\,cm} \geq +0.6$. Employing the results of Carilli & Yun (1999, 2000) and Dunne et al. (2000) leads to the conclusion that, once again, virtually all these sources (i.e. 18/19) must lie at redshifts greater than $\simeq 1.0$ (based on the mean values of $\alpha^{850\,\mu m}_{20\,cm}$; see Table 2). The mean redshift limit for the sample based on this $\alpha^{850\,\mu m}_{20\,cm}$ indicator is $\langle z_{\rm lim} \rangle = 1.5$.

Deeper radio observations of both fields are currently underway, and will be reported by Ivison et al. (in preparation).

3.4 175/850 μm flux-density ratio

When the 8-mJy survey was first designed it was anticipated that the *ISO* photo-polarimeter (ISOPHOT) 175-μm surveys of the two selected fields would yield a typical 3σ flux-density limit for undetected sources of $S_{175\,\mu m} < 50$ mJy. Such limits would be of considerable interest because, for a reasonable range of assumed SEDs, a non-detection of an 8-mJy SCUBA source at this 175-μm level would imply that $z > 2$. Unfortunately, in practice the ISOPHOT surveys have not come close to achieving their originally predicted sensitivities (failing by a factor of at least $\simeq 3$) and consequently the actual redshift constraints provided by the ISOPHOT coverage of our survey fields are generally weaker than those already derived above from the 450/850 and 20 cm/850 μm flux-density ratios. However, for completeness we note that the non-detection of all the ELAIS N2 sources in the 175-μm ELAIS survey ($S_{175\,\mu m} < 150$ mJy) does still imply a minimum redshift of $z > 1$ for all the SCUBA sources. This limit is included in column 5 of Table 2 as it does at least represent one further piece of independent evidence in support of the basic case that essentially all the bright SCUBA sources uncovered in the 8-mJy survey lie at $z > 1$.

Table 2. Current redshift information for the 19 most significant 850-μm sources from the 8-mJy SCUBA survey. Column 1 gives source names as defined in Scott et al. (2002). Column 2 lists spectroscopic redshifts for possible counterparts, currently available for two sources both for LH850.8 (Lehmann et al. 2001), see text for discussion of this object. Column 3 gives estimated redshift ranges and limits based on the redshift dependence of the radio–submm spectral index ($\alpha_{20\,\mathrm{cm}}^{850\,\mu\mathrm{m}}$; Carilli & Yun 1999, 2000). The $S_{1.4\,\mathrm{GHz}}$ upper limits are 4σ for the Lockman Hole (de Ruiter et al. 1997) and 5σ for the ELAIS N2 (Ciliegi et al. 1999) sources. Column 4 gives the ranges and limits on redshift derived from submm colour $S_{850\,\mu\mathrm{m}}/S_{450\,\mu\mathrm{m}}$ as illustrated in Fig. 3. Column 5 gives the crude lower redshift limits which follow from the failure to detect the SCUBA sources in 175-μm ISOPHOT maps. Finally, Column 6 gives the redshift ranges for four sources allowed by their detection at 1.2 mm with the MAMBO array at IRAM, providing interesting *upper* limits on redshift for these objects. The numbers in parentheses are the source references from Table 3.

Name	z_{spect}	$z(\alpha_{20\,\mathrm{cm}}^{850\,\mu\mathrm{m}})$	$z(S_{850\,\mu\mathrm{m}}/S_{450\,\mu\mathrm{m}})$	$z(S_{850\,\mu\mathrm{m}}/S_{175\,\mu\mathrm{m}})$	$z(S_{850\,\mu\mathrm{m}}/S_{1.2\,\mathrm{mm}})$
LH850.1	–	2–4	2–6	>1	0.5–5
LH850.2	–	>1.5	>1	–	–
LH850.3	–	>1.5	>2	–	–
LH850.4	–	>1.5	>1.5	–	–
LH850.5	–	>1.5	>1.5	–	–
LH850.6	–	>1.5	>2	–	–
LH850.7	–	>1.5	>1	–	–
LH850.8	–	>1.5	>1	>1	0–3
LH850.8 (1)	0.974	–	–	–	–
LH850.8 (2)	0.685	–	–	–	–
LH850.11	–	>1.5	0.5–3	–	–
LH850.12	–	0.5–2	>1	–	–
LH850.14	–	>1.5	>1	–	–
LH850.16	–	>1.5	>2	–	–
LH850.18	–	>1.5	>2	–	–
N2850.1	–	>1.5	2–7	>1	–
N2850.2	–	>1	1–5	>1	–
N2850.3	–	>1.5	>2.5	>1	–
N2850.4	–	>1.5	>1.5	>1	0–3
N2850.5	–	>1	>3	>1	–
N2850.7	–	>1.5	>1	>1	–

4 CANDIDATE OPTICAL, NEAR-INFRARED AND X-RAY COUNTERPARTS

4.1 Optical data

Deep *R*- and *I*-band images of the ELAIS N2 area were taken using the PFC on the WHT during 1999 and 2000 (Willott et al., in preparation), both covering 0.07 square degrees and reaching limiting depths of $R = 27$ and $I = 26$ (measured through a 1.5-arcsec radius aperture). An *I*-band image of the Lockman Hole E area has also been recently obtained with the PFC on the WHT (Ivison et al., in preparation), this time reaching a limiting depth of $I \simeq 24.5$. A deeper *I*-band image (reaching $I = 26$ through a 4-arcsec aperture) has also been obtained for LH850.1 and LH850.8.

Postage-stamp images have been extracted from these optical images, covering 30×30 arcsec centred on the position of each SCUBA source. These images are shown in Figs 4 and 5 (Lockman Hole), and in Fig. 6 (ELAIS N2) with the positional uncertainty for each SCUBA source indicated by a circle of radius 6 arcsec.

It is evident from these postage-stamp images that while for some SCUBA sources there exist no potential optical counterparts to the limit of these data, in most cases several alternative identifications lie within the SCUBA positional error circle. The positions of all optical sources within 6 arcsec of each 850-μm centroid are listed in Tables 3 and 4, with the corresponding aperture magnitudes (and in the case of empty fields, limiting magnitudes) included in Table 1.

The ambiguity surrounding the correct optical identification for most of the SCUBA sources is a result of the substantial uncertainty in the position of the 850-μm source, coupled with the large surface density of faint galaxies at the limiting magnitude of our deep optical data. To test whether any of these potential identifications are statistically compelling we have calculated, for every candidate object, the probability that a galaxy with the observed optical magnitude (or brighter) could lie so close to the SCUBA position by chance. The resulting probabilities (P_E; see Downes et al. 1986) are given for every candidate optical identification in Tables 3 and 4. We stress that these probabilities are often substantially higher than the raw Poisson probabilities (Downes et al. 1986). This is because the large search radius coupled with the high surface density of faint optical galaxies means that the vast majority of the SCUBA sources have at least one potential optical counterpart.

Unsurprisingly, the values of P_E derived for all but one the potential optical identifications are not, at this stage, compellingly small ($P_E < 0.05$). This result in part re-affirms the importance of future deeper radio and millimetre interferometric observations for reducing the search radius for potential counterparts. However, the current calculations are still of importance because they quantify the fact that at most one of the SCUBA sources (N2850.1) can be statistically associated with even a moderately bright optical counterpart. This result in itself provides further (completely independent) support for the conclusion arrived at above on the basis of SED constraints, that essentially all the SCUBA sources uncovered by the 8-mJy survey lie at $z > 1$.

It is interesting to consider in more detail the significance of the one statistically convincing optical identification uncovered by this analysis, namely that provided by both the *I* and *R*-band imaging of N2850.1. As can be seen from Table 4 and Fig. 6, the *R*-band image of this object provides 3 potential counterparts within the SCUBA position error circle. The brightest of these lies almost exactly on top of the nominal 850-μm position, while the two fainter options lie right at the edge of the adopted search region. Consequently, the brightest candidate has a very low probability of being a chance coincidence ($P_E = 0.06$), and indeed the probability of this object being a chance coincidence in the associated *I*-band image is even smaller ($P_E = 0.01$). Thus, unless future interferometric follow-up

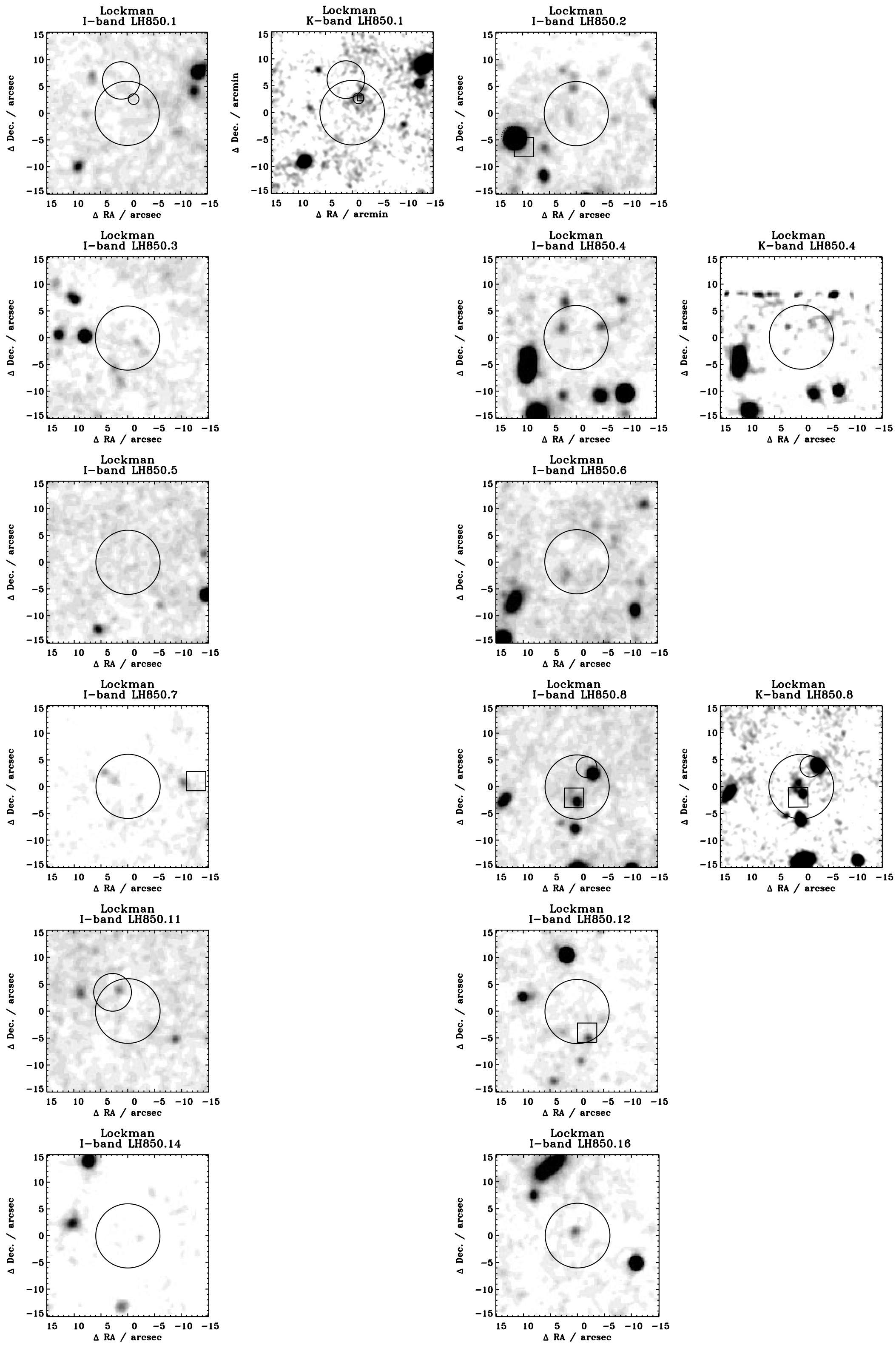

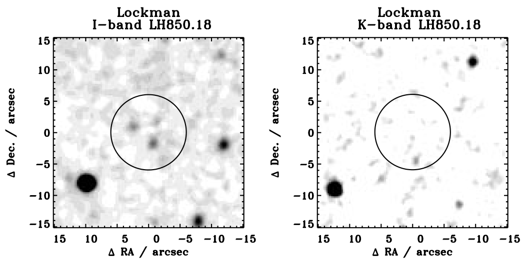

Figure 5. *I*- and *K*-band 30 × 30 arcsec postage stamps, centred on the 850 μm position of the Lockman Hole SCUBA source LH850.18, indicating potential optical and/or near-infrared counterparts to the source uncovered at 850 μm. The large circle in each figure has a radius of 6 arcsec, and defines the search radius adopted for the calculation of the statistical significance of each potential identification as described in Section 4.1.

should show the SCUBA position of this source to be seriously in error, it seems highly likely that this *RI*-band counterpart is physically associated with the 850-μm source. However, we would caution that this does not necessarily in itself guarantee that this is the correct identification, a point which is well demonstrated by the follow-up observations of the brightest submm source uncovered by Hughes et al. (1998) in the SCUBA image of the *Hubble Deep Field*. HDF 850.1 lies sufficiently close (≃ 1 arcsec distant) to the elliptical galaxy 3-586.0 that, as pointed out by Downes et al. (1998), the probability that this positional coincidence should occur by chance is $P_E = 0.05$, similar to the value derived here for N2850.1. However, despite this, subsequently improved astrometry provided by the IRAM Plateau de Bure interferometer (PdB) and VLA imaging of HDF 850.1 (Downes et al. 1999) has not strengthened the case for this possible identification. Indeed, based on broadband optical-infrared photometry, 3-586.0 appears to be a very passive elliptical at $z \simeq 1.1$, a redshift which is completely at odds with that inferred for the SCUBA source from SED constraints. Thus, at least in the case of HDF 850.1 it appears that a low value of P_E has been produced not because 3-586.0 is the correct identification, but perhaps because it is associated in some other way with the SCUBA source, possibly assisting its submm detectability via gravitational lensing. It will therefore be interesting to see whether further deeper observations of N2850.1 confirm the apparently convincing identification presented here, or reveal a more complex picture analogous to HDF 850.1.

Finally, we note that at this stage of the survey there are three SCUBA sources associated with *optical* blank fields; LH850.1 has no candidate identifications to a depth of $I = 27.4$, while LH 850.5 and LH850.14 have no possible optical counterparts to a depth of $I = 24.5$. These 3 objects are therefore particularly strong candidates for highly obscured, high-redshift galaxies, and in fact LH850.1 has now been discovered (via IRAM PdB 1.2-mm interferometry combined with very deep UKIRT *K*-band imaging) to be a faint and complex extremely red object (ERO) at $z \simeq 3$ (Lutz et al. 2001).

This discovery reinforces our confidence that (because of our conservative selection criteria) the lack of any potential optical counterparts for LH850.5 and LH850.14 reflects the nature and/or the remoteness of these galaxies, and should not be regarded as casting doubt on the reality of the 850-μm sources.

4.2 Near-infrared data

We have observed the central region of our Lockman Hole SCUBA survey area with the infrared camera INGRID mounted on the WHT, producing a single 4 × 4 arcmin *K*-band image. Figs 4 and 5 include 30 × 30 arcsec *K*-band postage stamps extracted from this image for the four 850-μm detections which fall within this area. A smaller but substantially deeper *K*-band image taken with UFTI on UKIRT (Lutz et al. 2001) has revealed new faint possible near-infrared counterparts for LH850.1 and LH 850.8. The *K*-band counterpart of LH850.1 has a magnitude of $K = 21.4$ (within a 1.5-arcsec radius aperture), and is located less than 1 arcsec from the refined position of the SCUBA source provided by its detection at 1.2 mm by the IRAM PdB interferometer. There is no doubt that this faint, red and apparently complex object is the correct identification for the SCUBA source (Lutz et al. 2001). For bright sources such as LH 850.1, lensing would be a more common event if the counts are steep at brighter fluxes.

The *K*-band image of LH850.8 is also of interest because it provides a third potential identification in addition to the two alternatives provided by the *I*-band image. This is a particularly complex source; the SCUBA error circle contains *ROSAT* X-ray source [LH850.8(1)] and VLA radio detection [LH850.8(2)], which appear to have distinct optical/IR counterparts, neither of which is necessarily a convincing identification for the SCUBA source. The radio source is VLA source 75 (according to the naming scheme of de Ruiter et al. 1997), and its VLA positional error box is shown in Fig. 4 to lie within the SCUBA error circle, coincident with one of the *K*-band sources. In fact de Ruiter et al. (1997) list this VLA source as a confident association with the *ROSAT* source 33. However, this association was based on the *ROSAT* Position Sensitive Proportional Counter (PSPC) centroid position which has poor spatial resolution. Subsequent observations with the High Resolution Imager (HRI) instrument, which has a much higher spatial resolution, indicate that *ROSAT* source 33 is associated with the upper *K*-band source as illustrated in Fig. 4 and not with the VLA detection (Lehmann et al. 2001). Recent optical spectroscopy of the VLA source by Lehmann (private communication) has revealed LH850.8(2) to be an emission line galaxy at $z = 0.685$. If the submm source and the VLA source are

Figure 4. *I*- and *K*-band 30 × 30 arcsec postage stamps, centred on the 850-μm positions of the Lockman Hole SCUBA sources, indicating potential optical and/or near-infrared counterparts to the sources uncovered at 850 μm. The large circle in each figure has a radius of 6 arcsec, and defines the (conservatively large) search radius adopted for the calculation of the statistical significance of each potential identification as described in Section 4.1. Top-left is LH850.1, which is the most significant 850-μm source in our sample, and has been the subject of detailed follow-up by Lutz et al. (2001). In this case an additional 3-arcsec radius circle is included centred on the position of our 450-μm detection, with an even smaller circle (1-arcsec radius) centred on the position yielded by the 1.2-mm IRAM PdB interferometric detection of Lutz et al. (2001). The position of the 450-μm detection of LH850.11 is also marked, a position which arguably increases the possibility of the single optical counterpart provided by the *I*-band image. For LH850.7, LH850.8 and LH850.12, boxes have been included to indicate the 2σ positional uncertainty associated with the nearest radio sources found in the VLA survey of de Ruiter et al. (1997). For LH850.8, the position of the X-ray source (denoted as LH850.8(1) in Tables 1, 2 and 3) detected via *ROSAT* HRI imaging has also been marked (small circle). The picture for this object is particularly complex/confusing, with the radio source being strongly associated with one potential optical/IR SCUBA ID, while the X-ray source is apparently associated with another. However, neither optical object is in itself a statistical compelling counterpart to the 850-μm source.

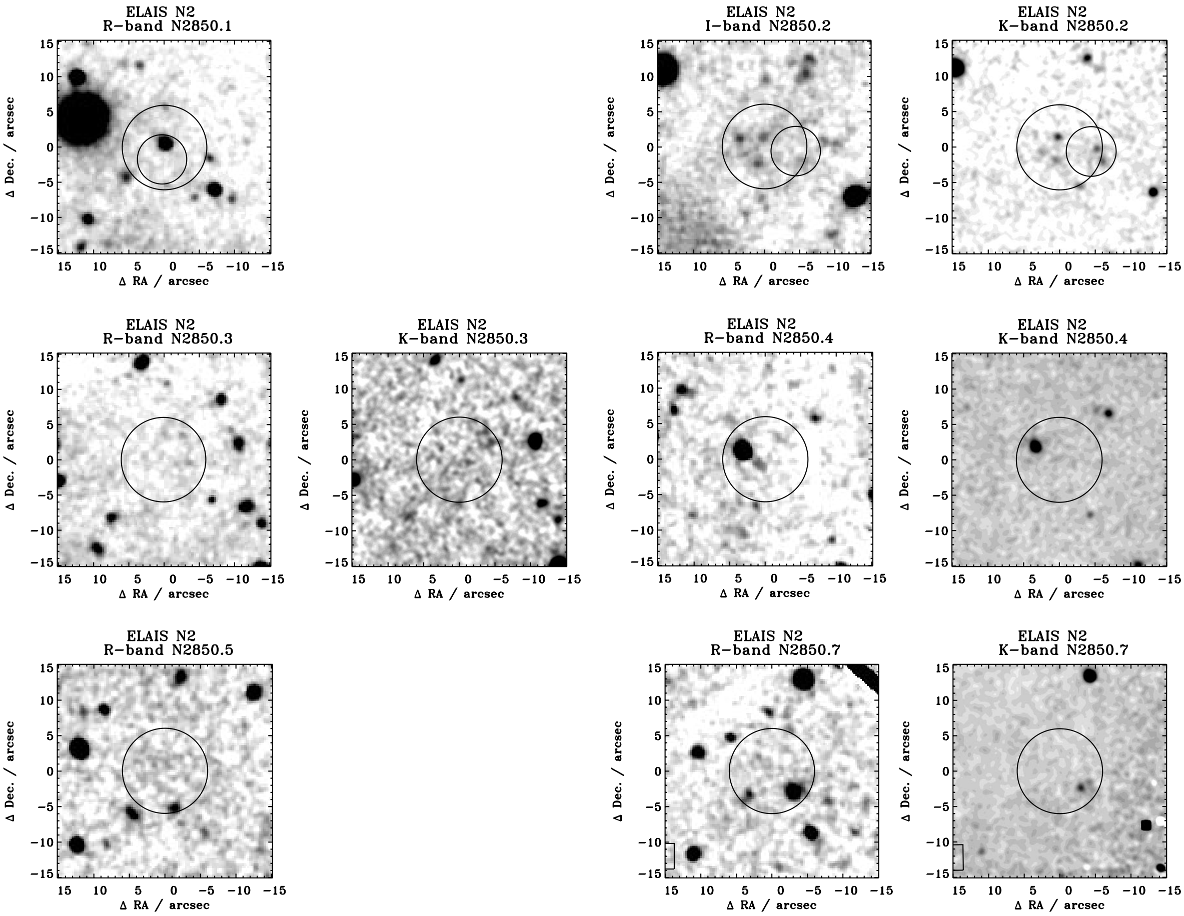

Figure 6. *R*- and *K*-band 30×30 arcsec postage stamps, centred on the 850 μm positions of the ELAISN2 SCUBA sources, indicating potential optical and/or near-infrared counterparts to the sources uncovered at 850 μm. The large circle in each figure has a radius of 6 arcsec, and defines the search radius adopted for the calculation of the statistical significance of each potential identification as described in Section 4.1. Two sources, N2850.1 and N2850.2, have significant 450-μm detections the positions of which, as in Fig. 4, are indicated by circles with a radius of 3 arcsec. In the case of N2850.1, the position of the 450-μm source reinforces the likelihood that the statistically compelling optical/IR identification centred on the 850-μm position is correct. However, in the case of N2850.2 the 450-μm position points towards one of the red objects seen only in the *K*-band image (near the western edge of the 850-μm error circle) as the most likely identification.

indeed physically associated, the spectrocopic redshift is consistent with broad range ($z = 0.5 - 3$) derived from the Carilli & Yun (2000) indicator.

Our new, deep *K*-band image of this region has now revealed a third, faint ($K = 20.2$) infrared source north-east of the VLA source [denoted as LH850.3(3)], close to the 850-μm centroid but outside the VLA error box. The non-detection of this source in the *I*-band image indicates that it is red, with $I - K > 4.28$ which, given our experience with LH850.1, strengthens our conviction that this is probably the true SCUBA identification, despite the fact that the P_E statistic marginally favours the VLA source as the least likely chance association. Table 2 lists the redshift limits of LH850.8 with no assumptions of the true counterpart and also the two spectroscopically derived redshifts. Deep, high-resolution IRAM imaging will resolve this conundrum. LH850.8 will be discussed further in Ivison et al. (in preparation).

A substantial fraction of our ELAIS N2 survey field has now also been mapped in the *K*-band, in this case with the UFTI camera on UKIRT. This dataset comprises 13 individual frames, each covering a field approximately 100×100 arcsec in size. Typical exposure times are 120 min per pointing, resulting in images which reach a 3-σ detection limit of $K \simeq 21.5$ as measured with a 1.5-arcsec radius aperture. One frame containing two strong SCUBA detections has been imaged to an increased depth of $K \simeq 22$. Of the six bright SCUBA sources in the ELAIS N2 region, two (N2850.1 and N2850.5) unfortunately lie outside the field covered by this deep *K*-band mosaic. *K*-band postage stamps covering 30×30 arcsec are provided for the remaining four sources in Fig. 6.

A number of SCUBA sources have now been convincingly shown to be associated with EROs with $R - K > 5$ (Smail et al. 1999; Frayer et al. 2000; Ivison et al. 2000). Consequently, particularly in the light of our own detailed study of LH850.1 (Lutz et al. 2001), we have good reason for taking particularly seriously any potential SCUBA identifications revealed in *K*-band images which transpire to be extremely faint, or undetected in the complementary optical data (Ivison et al., in preparation). Three of four SCUBA galaxies from the lensing cluster survey were initially named as being associated with brighter optical counterparts until deeper near-IR imaging revealed the fainter, redder sources classing them as EROs (Smail et al. 1999; Frayer et al. 2000). In addition to the cases of LH850.1 and LH850.8 discussed above, the possible *K*-band counterparts of three ELAIS N2 sources are EROs with $R - K > 5.3$, $R - K > 5.8$ and $R - K > 6$ for N2850.2(3),

Table 3. Positions of SCUBA sources and possible optical/infrared/radio/X-ray counterparts in the Lockman Hole E area. Column 2 shows detections close to the SCUBA centroid. The positional errors are typically ±0.1–0.2 arcsec for the *R*-, *I* and *K*-band sources, ±2 arcsec for the VLA sources and ±2 arcsec for the SCUBA 450-μm sources. The P_E statistic (outlined in the text) quantifies the probability that the optical or infrared counterpart may be a chance coincidence (Section 4.1).

Catalogue name		RA α_{2000} ($^{h\ m\ s}$)	Dec δ_{2000} ($^{\circ\ \prime\ \prime\prime}$)	Note
LH850.1	SCUBA 850 μm	10 52 01.439	+57 24 43.15	7.62 S/N
	SCUBA 450 μm	10 52 01.577	+57 24 49.30	3.82 S/N
	IRAM PdB 1.2 mm	10 52 01.284	+57 24 45.94	Lutz et al. 2001
	K-band Peak	10 52 01.300	+57 24 46.00	Lutz et al. 2001
	VLA 1.4 GHz	10 52 01.249	+57 24 45.88	Ivison et al., in preparation
LH850.2	SCUBA 850 μm	10 52 38.214	+57 24 36.10	4.70 S/N
	I-band Peak	10 52 38.280	+57 24 40.93	$P_E = 0.40$
LH850.3	SCUBA 850 μm	10 51 58.272	+57 18 01.14	4.93 S/N
	I-band Peak	10 51 58.536	+57 17 55.68	$P_E = 0.46$
LH850.4	SCUBA 850 μm	10 52 04.138	+57 25 28.15	5.14 S/N
	I-band Peak (1)	10 52 04.440	+57 25 29.96	$P_E = 0.21$
	K-band Peak (1)	10 52 04.222	+57 25 31.04	$P_E = 0.60$
	I-band Peak (2)	10 52 03.528	+57 25 30.25	$P_E = 0.22$
	K-band Peak (2)	10 52 03.647	+57 25 31.73	$P_E = 0.54$
	K-band Peak (3)	10 52 03.959	+57 25 30.46	$P_E = 0.55$
LH850.5	SCUBA 850 μm	10 51 59.341	+57 17 17.65	4.50 S/N
LH850.6	SCUBA 850 μm	10 52 30.582	+57 22 11.59	4.24 S/N
	I-band Peak	10 52 30.792	+57 22 09.59	$P_E = 0.23$
LH850.7	SCUBA 850 μm	10 51 51.456	+57 26 35.12	4.34 S/N
	I-band Peak	10 51 51.984	+57 26 37.93	$P_E = 0.44$
LH850.8	SCUBA 850 μm	10 51 59.969	+57 24 21.29	4.26 S/N
	ROSAT HRI (1)	10 52 00.0	+57 24 24.50	Lehmann et al. 2001
	R-band Peak (1)	10 52 00.0	+57 24 26.10	Lehmann et al. 2001
	I-band Peak (1)	10 51 59.832	+57 24 24.91	$P_E = 0.12$
	K-band Peak (1)	10 51 59.905	+57 24 25.30	$P_E = 0.54$
	VLA 1.4 GHz(2)	10 52 00.29	+57 24 20.3	de Ruiter et al. 1997
	I-band Peak (2)	10 52 00.192	+57 24 19.69	$P_E = 0.11$
	K-band Peak (2)	10 52 00.242	+57 24 19.97	$P_E = 0.28$
	K-band Peak (3)	10 52 00.289	+57 24 22.97	$P_E = 0.61$
LH850.11	SCUBA 850 μm	10 51 30.601	+57 20 38.48	4.43 S/N
	SCUBA 450 μm	10 51 30.949	+57 20 41.95	3.78 S/N
	I-band Peak	10 51 30.792	+57 20 42.50	$P_E = 0.40$
LH850.12	SCUBA 850 μm	10 52 07.723	+57 19 06.65	4.03 S/N
	I-band Peak	10 52 07.464	+57 19 01.70	$P_E = 0.40$
	VLA 1.4 GHz	10 52 07.49	+57 19 02.7	de Ruiter et al. 1997
	I-band Peak	10 52 08.016	+57 19 02.93	$P_E = 0.40$
LH850.14	SCUBA 850 μm	10 52 04.298	+57 26 59.16	4.64 S/N
LH850.16	SCUBA 850 μm	10 52 27.080	+57 25 16.23	4.15 S/N
	I-band Peak	10 52 27.120	+57 25 17.18	$P_E = 0.04$
LH850.18	SCUBA 850 μm	10 51 55.661	+57 23 12.14	4.46 S/N
	I-band Peak (1)	10 51 55.560	+57 23 10.43	$P_E = 0.15$
	I-band Peak (2)	10 51 55.944	+57 23 13.06	$P_E = 0.24$

N2850.3(3) and N2850.7(3), respectively. Extrapolating the ERO number counts of Daddi et al. (2000) to the *K*-band limit of 21.5 for $R - K > 6$ yields an estimated expected ERO density of 0.5 square arcmin^{-1}. By chance we would thus expect only ~0.1 EROs to fall within the 6-arcsec search radius in *one* of the eight possible fields for which we possess *K*-band imaging. Thus, the relative rarity of such red objects strengthens the argument that these EROs are indeed the correct identifications for the SCUBA sources. However, it must be acknowledged that the estimated ERO source density below $K \sim 20$ is a source of large uncertainty.

4.3 X-ray data

As mentioned above the SCUBA source, LH850.8 is only 4.8-arcsec distant from an X-ray source detected in the *ROSAT* deep survey (Hasinger et al. 1998; Lehmann et al. 2001) here named LH 850.8(1). Deep *R*-band imaging and optical spectroscopy has been obtained for the optical counterpart of this X-ray source [No. 33, using the Lehmann et al. (2000) naming scheme] by Lehmann et al. (2000). The spectrum displays narrow O II and Ne V emission and a broad Mg II line, revealing this object to be an AGN at $z = 0.9$.

The proximity of this AGN to the SCUBA source LH850.8 is undeniably interesting but, as discussed above, neither this source nor the nearby VLA radio source [LH850.8(2)] can be unambiguously associated with the SCUBA source. At present we therefore have no compelling evidence for AGN activity in any of the 19 bright SCUBA sources considered here.

However, deep Chandra observations in the field of Abell 370 by Bautz et al. (2000) have revealed hard X-ray sources coincident with SCUBA sources and suggest that around 20 per cent of the submm population may have a significant contribution from an AGN component.

Fabian et al. (2000) and Barger et al. (2001a,b) have found a similarly low submm detection rate with X-ray samples; the contribution to the 850-μm background light from hard X-ray

Table 4. Positions of SCUBA sources and possible optical-infrared counterparts in the ELAIS N2 area. Column 2 shows detections close to the SCUBA centroid. The positional errors are typically ±0.1–0.2 arcsec for the R, I and K-band sources, ±2 arcsec for the VLA sources and ±2 arcsec for the SCUBA 450-μm sources. The P_E statistic (outlined in the text) quantifies the probability that the optical or infrared counterpart may be a chance coincidence (Section 4.1).

Catalogue name		RA α_{2000} ($^{\mathrm{h\ m\ s}}$)	Dec δ_{2000} ($^{\circ\ \prime\ \prime\prime}$)	Note
N2850.1	SCUBA 850 μm	16 37 04.332	+41 05 30.32	8.46 S/N
	SCUBA 450 μm	16 37 04.363	+41 05 28.64	4.24 S/N
	R-band Peak (1)	16 37 04.343	+41 05 31.24	$P_E = 0.06$
	I-band Peak (1)	16 37 04.331	+41 05 30.72	$P_E = 0.01$
	R-band Peak (2)	16 37 04.684	+41 05 34.57	$P_E = 0.93$
	R-band Peak (3)	16 37 04.315	+41 05 25.20	$P_E = 0.94$
N2850.2	SCUBA 850 μm	16 36 58.651	+41 05 24.35	6.05 S/N
	SCUBA 450 μm	16 36 58.260	+41 05 23.70	3.60 S/N
	R-band Peak	Diff Spikes		
	I-band Peak (1)	16 36 58.662	+41 05 25.71	$P_E = 0.23$
	K-band Peak (1)	16 36 58.682	+41 05 25.76	$P_E = 0.33$
	I-band Peak (2)	16 36 58.731	+41 05 21.87	$P_E = 0.54$
	K-band Peak (2)	16 36 58.704	+41 05 22.60	$P_E = 0.45$
	K-band Peak (3)	16 36 58.198	+41 05 24.04	$P_E = 0.92$
	I-band Peak (4)	16 36 58.884	+41 05 23.32	$P_E = 0.74$
	K-band Peak (4)	16 36 58.872	+41 05 23.67	$P_E = 0.68$
	I-band Peak (5)	16 36 58.963	+41 05 25.49	$P_E = 0.67$
N2850.3	SCUBA 850 μm	16 36 58.228	+41 04 42.35	6.16 S/N
	R-band Peak (1)	16 36 58.083	+41 04 41.98	$P_E = 0.47$
	I-band Peak (1)	16 36 58.060	+41 04 41.55	$P_E = 0.50$
	R-band Peak (2)	16 36 57.925	+41 04 42.39	$P_E = 0.77$
	K-band Peak (3)	16 36 57.839	+41 04 44.79	$P_E = 0.94$
N2850.4	SCUBA 850 μm	16 36 50.143	+40 57 32.87	5.70 S/N
	R-band Peak (1)	16 36 50.180	+40 57 32.10	$P_E = 0.20$
	R-band Peak (2)	16 36 50.435	+40 57 34.46	$P_E = 0.34$
	I-band Peak (2)	16 36 50.433	+40 57 34.54	$P_E = 0.32$
	K-band Peak (2)	16 36 50.424	+40 57 34.88	$P_E = 0.44$
	R-band Peak (3)	16 36 50.258	+40 57 32.64	$P_E = 0.31$
N2850.5	SCUBA 850 μm	16 36 35.624	+40 55 57.86	5.64 S/N
	R-band Peak	16 36 35.518	+40 55 53.05	$P_E = 0.85$
	I-band Peak	16 36 35.528	+40 55 52.87	$P_E = 0.88$
N2850.7	SCUBA 850 μm	16 36 39.415	+40 56 38.37	5.37 S/N
	R-band Peak (1)	16 36 39.155	+40 56 35.93	$P_E = 0.56$
	I-band Peak (1)	16 36 39.174	+40 56 35.87	$P_E = 0.45$
	K-band Peak (1)	16 36 39.144	+40 56 35.96	$P_E = 0.70$
	R-band Peak (2)	16 36 39.713	+40 56 35.50	$P_E = 0.84$
	I-band Peak (3)	16 36 39.052	+40 56 36.96	$P_E = 0.76$
	K-band Peak (3)	16 36 39.049	+40 56 36.53	$P_E = 0.92$

sources estimated from these works to be lower; around 10 per cent.

These results suggest that deeper X-ray imaging of the 8-mJy survey might also be expected to yield some convincing X-ray detections of our SCUBA sources.

In fact, a deep Chandra image of the ELAIS N2 field has now been obtained, and an analysis of the cross-correlation between the faint X-ray population and the SCUBA sources based on the 8-mJy survey will be the subject of a forthcoming paper by Almaini et al. (2001).

5 DISCUSSION

Determining the redshift distribution of the submm-selected galaxy population is now regarded as a key goal in observational cosmology. This is of importance for assessing the contribution of dust-enshrouded star formation activity to overall star formation density at high redshift, and for determining whether the massive starbursts which power these objects are spread throughout much of cosmic history, or mainly confined to a relatively short-lived epoch. Division of submm-selected samples into (even crude) redshift bands will also be of importance for refining current measurements of submm source clustering (Scott et al. 2002), measurements which have the potential to settle the issue of whether bright submm sources are the high-redshift progenitors of present-day massive ellipticals.

Given the growing evidence that many, and perhaps most, submm sources have very faint, often red optical/IR identifications, it seems clear that the measurement of spectroscopic redshifts for significant numbers of SCUBA sources will be a long-term project. Indeed, for some sources such measurements may not be feasible until the advent of deep infrared spectroscopy with NGST, or broad-band millimetre spectroscopy with ALMA or the Large Millimetre Telescope (LMT).

Therefore, as stressed in the introductory section of this paper, while not losing sight of the ultimate goal of spectroscopic redshifts, it is important to recognize what can be learned about the redshifts of submm sources using currently operational facilities. In particular it seems likely that, to the first order, the basic redshift distribution of the submm source population can be derived from broad-band radio–submm photometric constraints, coupled with the study of potential counterparts revealed by deep optical and near-infrared imaging. However, the usefulness of such techniques has until now been hampered by the lack of a substantial and unbiased sample of submm-selected sources of sufficient luminosity to allow detection of the majority of the 850-μm sources at other wavelengths (e.g. radio, millimetre and far-infrared wavelengths).

It is of course important to recognize that a meaningful sample of apparently bright submm sources has been provided by SCUBA observations of lensing clusters (Smail et al. 1997), and that the extensive follow-up of these sources (Ivison et al. 1998, 2000; Frayer et al. 1998, 1999, 2000) has produced great strides in our knowledge of the submm population. The lensing strategy is not without problems, however. For example, the small fields of view severely hamper measures of the clustering properties (if any) of SCUBA sources.

With completion of 850-μm source extraction from the 8-mJy SCUBA survey (Scott et al. 2002) we now, for the first time, possess the required statistically meaningful and unbiased sample of bright submm sources. The results reported here thus represent an important step towards measuring the redshift distribution of the luminous submm galaxy population.

The key result of this work is that the SED-based redshift constraints, in particular the more powerful constraints provided by the combination of the 850-μm, 450-μm and 20-cm data, all point to the same conclusion that essentially all of the 8-mJy sources lie at $z > 1$ and that at least half appear to lie at $z > 2$. At the same time the upper limits on redshift, where available, do not violate these minimum redshift constraints but suggest that not many of the sources are likely to lie at very extreme redshifts ($z > 4$). We have also demonstrated that candidate optical and/or near-infrared counterparts, while rarely offering unambiguous identifications given the current positional uncertainties, are certainly consistent with the SED-based redshift estimates.

These redshift constraints may appear crude, but nonetheless are potentially very significant. In particular they confirm that most of the star formation which occurs in very extreme starbursts (SFR > $1000\,M_{\odot}\,yr^{-1}$) is confined to the first 2–3 Gyr of the history of the universe. The stellar populations produced by this population must therefore appear highly coeval and typically >10 Gyr old by the present day, strengthening the argument that high-redshift submm sources are the progenitors of present-day evolved ellipticals. Moreover, these redshift bounds also confirm the plausibility of the redshift ranges adopted by Scott et al. (2002) for the estimation comoving number density of luminous dust-enshrouded starbursts in the young universe. This calculation which yields a value comparable to the present-day comoving number density of luminous ($L > 3L^*$) ellipticals, $\simeq 1 \times 10^{-5}\,\mathrm{Mpc}^{-3}$, provides further (albeit circumstantial) support for the plausibility of the evolution of faint submm source into a present-day massive elliptical.

The other most interesting result of the analysis presented in this paper is the tantalizing suggestion that a large fraction of very luminous submm sources may transpire to be associated with faint EROs. Specifically, while at present we only possess deep *K*-band images of eight of the 19 most significant 850-μm sources, five out of these eight images have revealed a potential ERO counterpart to the SCUBA source. In the case of LH850.1 the validity of this association has now been demonstrated beyond doubt, and the relative rarity of EROs in the field adds further credence to the other possible ERO associations. Thus, while the overall SCUBA population may contain a wide range of different classes of object, it seems possible that a substantial fraction of the brightest SCUBA sources sampled by the 8-mJy survey may well be EROs. Deeper VLA observations of our survey fields have the potential to yield much more accurate positions for a substantial fraction of the 8-mJy sources, and are thus expected to clarify which of the potential optical/IR identifications highlighted in the previous section can indeed be reliably associated with the SCUBA sources (Ivison et al., in preparation).

6 CONCLUSIONS

In summary, the main results and conclusions of the SCUBA 8-mJy survey are:

(i) All of the faint SCUBA sources detected in this survey lie at $z > 1$ and at least 50 per cent appear to lie at $z > 2$.

(ii) The SED-derived redshift limits and ranges agree with the extreme star formation rates ($>1000\,M_{\odot}\,yr^{-1}$) for SCUBA sources calculated in Scott et al. (2002).

(iii) For the SCUBA sources for which we have deep near infrared data there are strong indications that EROs and faint SCUBA sources are physically associated.

ACKNOWLEDGMENTS

The authors wish to thank Thomas Greve for the reduction of the *I*-band imaging of the Lockman Hole field, along with Dieter Lutz and Andrew Baker for undertaking and reducing the 1.2-mm photometry measurements made with the IRAM 30-m telescope. The authors would also like to thank Ingo Lehmann for additional spectra from the follow-up of *ROSAT* deep survey. MF, AE, SuS, StS, BM, SO and CW all acknowledge the support of PPARC during the course of this project. OA acknowledges the support of the Royal Society, while JD acknowledges the enhanced research time afforded by the award of a PPARC Senior Fellowship. The JCMT is operated by the Joint Astronomy Centre on behalf of the UK Particle Physics and Astronomy Research Council, the Canadian National Research Council and the Netherlands Organization for Scientific Research. The UKIRT is operated by the Joint Astronomy Centre on behalf of the UK Particle Physics and Astronomy Research Council. The WHT is operated by the Isaac Newton Group on behalf of the UK Particle Physics and Astronomy Research Council and the Netherlands Organization for Scientific Research.

REFERENCES

Almaini O. et al., 2001, MNRAS, submitted (astro-ph/0108400)
Baker A., Lutz D., Genzel R., Tacconi L. J., Lehnert M. D., 2001, A&A, 372, L37
Barger A. J., Cowie L. L., Sanders D. B., Fulton E., Taniguchi Y., Sato Y., Kamara K., Okuda H., 1998, Nat, 394, 248
Barger A. J., Cowie L. L., Sanders D. B., 1999a, ApJ, 518, L5
Barger A. J., Cowie L. L., Smail I., Ivison R. J., Blain A. W., Kneib J. P., 1999b, AJ, 117, 2656
Barger A. J., Cowie L. L., Richards E. A., 2000, AJ, 119, 2092
Barger A. J., Cowie L. L., Mutshotsky R. F., Richards E. A., 2001a, AJ, 121, 662
Barger A. J., Cowie L. L., Steffen A. T., Hornschemeier A. E., Brandt W. N., Garmire G. P., 2001b, ApJ, 560, L23
Bautz M. W. et al., 2000, ApJ, 543, L119
Bertoldi F. et al., 2000, A&A, 360, 92
Blain A. W., Longair M. S., 1996, MNRAS, 279, 847

Blain A. W., Knieb J. P., Ivison R. J., Smail I., 1999, ApJ, 512, L87
Carilli C. L., Yun M. S., 1999, ApJ, 513, L13
Carilli C. L., Yun M. S., 2000, ApJ, 530, 1024
Chapman S. C., Richards E. A., Lewis G. F., Wilson G., Barger A. J., 2001, ApJ, 548, L147
Ciliegi P. et al., 1998, MNRAS, 302, 222
Condon J. J., 1992, ARA&A, 30, 575
Daddi E., Cimatti A., Pozzetti L., Hoekstra H., Röttgering H. J. A., Renzini A., Zamorani G., Mannucci F., 2000, A&A, 361, 535
Dey A. et al., 1999, ApJ, 519, 610
Dole H. et al., 2001, A&A, 372, 364
Downes A. J. B., Peacock J. A., Savage A., Carrie D. R., 1986, MNRAS, 218, 31
Downes D. et al., 1999, A&A, 347, 809
Dunlop J. S., 2001, in van Bemmel I. M., Wilkes B., Barthel P., eds, FIRSED, New Astron. Rev. Elsevier, Amsterdam, 45, 609
Dunne L., Clements D., Eales S. A., 2000, MNRAS, 319, 813
Eales S. A., Lilly S. J., Gear W. K., Bond J. R., Dunne L., Hammer F., Le Fevre O., Crampton D., 1999, ApJ, 515, 518
Eales S. A., Lilly S. J., Webb T., Dunne L., Gear W., Clements D., Yun M., 2000, AJ, 120, 2244
Efstathiou A., Rowan-Robinson M., Siebenmorgen R., 2000, MNRAS, 313, 734
Fabian A. C. et al., 2000, MNRAS, 315, L8
Farrah D. et al., 2001, MNRAS, 326, 1333
Frayer D. T., Ivison R. J., Scoville N. Z., Yun M., Evans A. S., Smail I., Blain A. W., Kneib J.-P., 1998, ApJ, 506, L7
Frayer D. T. et al., 1999, ApJ, 514, L13
Frayer D. T., Smail I., Ivison R. J., Scoville N. Z., 2000, AJ, 120, 1668
Gear W. K., Lilly S. J., Stevens J. A., Clements D. L., Webb T. M., Eales S. A., Dunne L., 2000, MNRAS, 316, L51
Hasinger G., Burg R., Giacconi R., Schmidt M., Trumper J., Zamorani G., 1998, A&A, 329, 482
Helou G., Soifer B. T., Rowan-Robinson M., 1985, ApJ, 298, L7
Hornshemeier et al., 2000, ApJ, 554, 742
Hughes D. H., Dunlop J. S., 1998, in Carilli C. L., ed., ASP Conf. Ser. Vol. 156, High Redshift Radio Lines. Astron. Soc. Pac., San Francisco, p. 99
Hughes D. H. et al., 1998, Nat, 394, 241
Ivison R. J., Smail I., Le Borgne J.-F., Blain A. W., Kneib J.-P., Bezecourt J., Kerr T. H., Davies J. K., 1998, MNRAS, 298, 583
Ivison R. J., Smail I., Barger A. J., Knieb J. P., Blain A. W., Owen F. N., Kerr T. H., Cowie L. L., 2000, MNRAS, 315, 209
Kreysa E. et al., 1998, Proc. SPIE, 3357, 319
Lehmann I. et al., 2000, A&A, 354, 35
Lehmann I. et al., 2001, A&A, 371, 833
Lilly S. J. et al., 1999, ApJ, 518, 641
Lutz D. et al., 2001, A&A, 378, 70
Oliver S. et al., 2000, MNRAS, 316, 749
Peacock J. A. et al., 2000, MNRAS, 318, 535
Puget J.-L. et al., 1999, A&A, 345, 29
Rowan-Robinson M. et al., 1997, MNRAS, 289, 490
Rowan-Robinson M., 2001, ApJ, 549, 745
de Ruiter H. R. et al., 1997, A&A, 319, 7
Sanders D. B., Mirabel I. F., 1996, ARA&A, 34, 749
Schmidt M. et al., 1998, A&A, 329, 495
Scott S. E. et al., 2002, MNRAS, 331, 817 (this issue)
Serjeant S. et al., 2000, MNRAS, 316, 768
Serjeant S. et al., 2002, MNRAS, submitted (astro-ph/0201502)
Smail I., Ivison R. J., Blain A. W., 1997, ApJ, 490, L5
Smail I., Ivison R. J., Kneib J.-P., Cowie L. L., Blain A. W., Barger A. J., Owen F. N., Morrison G., 1999, MNRAS, 308, 1061
Smail I., Ivison R. J., Owen F. N., Blain A. W., Kneib J.-P., 2000, ApJ, 528, 612
Soucail G. et al., 1999, A&A, 343, L70
Townsend R. et al., 2001, MNRAS, preprint (astro-ph/0106112)

This paper has been typeset from a TEX/LATEX file prepared by the author.